Accepted Manuscript

Bipolar highly solid-state luminescent phenanthroimidazole derivatives as materials for blue and white organic light emitting diodes exploiting either monomer, exciplex or electroplex emission

Rita Butkutė, Ramūnas Lygaitis, Viktorija Mimaitė, Dalius Gudeika, Dmytro Volyniuk, Gjergji Sini, Juozas Vidas Grazulevicius

Please cite this article as: Butkutė R, Lygaitis Ramū, Mimaitė V, Gudeika D, Volyniuk D, Sini G, Grazulevicius JV, Bipolar highly solid-state luminescent phenanthroimidazole derivatives as materials for blue and white organic light emitting diodes exploiting either monomer, exciplex or electroplex emission, *Dyes and Pigments* (2017), doi: 10.1016/j.dyepig.2017.07.029.

Bipolar highly solid-state luminescent phenanthroimidazole derivatives as materials for blue and white organic light emitting diodes exploiting either monomer, exciplex or electroplex emission

Rita Butkutė[1], Ramūnas Lygaitis[1], Viktorija Mimaitė[1], Dalius Gudeika[1], Dmytro Volyniuk[1], Gjergji Sini[2], Juozas Vidas Grazulevicius[1]

[1]Department of Polymer Chemistry and Technology, Kaunas University of Technology, Radvilėnų pl. 19, LT-50254 Kaunas, Lithuania

[2] Laboratoire de Physicochimie des Polymères et des Interfaces, Université de Cergy-Pontoise, EA 2528, 5 mail Gay-Lussac, Cergy-Pontoise Cedex, 95031, France

Abstract

Four phenanthroimidazole-based bipolar compounds having electron-donating carbazole or diphenylamino moieties were synthesized and characterized. All compounds form glasses and exhibit high glass transition temperatures ranging from 183 to 239 $^{\circ}$C. Solid state blue emission was detected for all synthesized compounds and quantum yields in solid state reached 0.55. Room temperature hole and electron mobilities in the layers of phenanthroimidazole derivatives reached 3.14×10^{-4} and 5.69×10^{-4} cm^2/V·s, respectively, at an electric field of 3.6×10^5 V/cm. Quantum chemical calculations on the molecular level were employed to interpret optical, photophysical and photoelectrical properties of the compounds. Due to the efficient blue solid-state emission and ambipolar charge transport the phenanthroimidazole-based derivatives were used for the preparation of non-doped emitting layers of blue OLEDs. The electroplex forming properties of the compounds were observed in a host:guest emitting layer with a commercial hole-transporting material 4,4′-

cyclohexylidenebis[*N,N*-bis(4-methylphenyl)benzenamine]. Two most promising phenanthroimidazole-based compounds were used for the fabrication of white OLEDs which were based on both fluorescence and either electroplex or exciplex emissions. The best almost blue and white OLEDs were characterized by maximal current efficiency of 1.3 and 5.3 cd/A, power efficiency of 0.8 and 1.7 lm/W, and external quantum efficiency of 0.95 and 2.9 %.

Keywords. Phenanthroimidazole, solid-state emission, ambipolar mobility, exciplex, electroplex

1. Introduction

Intermolecular charge transfer systems enabling thermally activated delayed fluorescence (TADF) are utilized for the fabrication of organic light-emitting diodes (OLEDs). The possibility of emissive harvesting of 100 % excited states in the emitting layers based on such systems was discovered [1, 2]. The emissive harvesting of TADF occurs through the lowest singlet energy level to which energy is additionally transferred from the triplet energy level [1]. Interaction of holes on a highest occupied molecular orbital (HOMO) level of donor molecules with electrons on a lowest unoccupied molecular orbital (LUMO) level of acceptor molecules in a donor-acceptor molecular mixture leads to the formation of the intermolecular charge transfer systems [3,4,5].

Exciplex emission can be obtained from the donor-acceptor molecular mixtures under both photo- and electro-excitations [4]. The singlet and triplet energy levels are close for exciplex-forming compounds and this similarity leads to the reverse intersystem crossing (RISC) and, as a result, TADF can be obtained [6]. However, since the energy levels of exciplexes are always lower than singlet energies of exciplex-forming donor and acceptor molecules, the exciplex emission is shifted to lower-energy spectral region compared to the emission of pure donor and acceptor molecules [7,8]. Despite that, expedient selection of donor and acceptor molecules by carefully analysing their HOMO and LUMO energies allows to obtain exciplex emission with colours ranging from blue to red, which was successfully exploited in all-exciplex OLEDs of different colours including white

2

devices [3]. Exciplex-forming donor-acceptor mixtures are also exploited as hosts in phosphorescent OLEDs for energy transfer from an exciplex to an emitter [9]. White OLEDs with single emitting layer can be designed since interface exciplexes can be formed between compounds constituting neighbouring layers [9]. A vertical organic light-emitting transistor with adjustable emission colour was demonstrated using a periodic interrupted middle electrode in the region of an interface exciplex [10]. Recently, long-range coupling of electron-hole pairs which produce exciplexes in organic multilayer structures was observed [11]. This observation opens new possibilities in the development of efficient exciplex-based devices.

Another intermolecular charge transfer system, i.e. electroplex can also be formed between donor and acceptor molecules [3]. Electroplex emission can be observed only under electrical excitation through carrier recombination of holes on a HOMO level of donor and of electrons on a LUMO level of acceptor [12]. Electroplex emission can be utilized as a good approach for the fabrication of OLEDs similarly to exciplex emission. For example, a white top-emitting OLED with a single emissive layer based on an interface electroplex between low-molar-mass compounds 4,4' - bis(2,2'-diphenylvinyl)-1,1'-biphenyl (DPVBi) and 2,9-dimethyl-4,7- diphenyl-1,1'-phenanthroline (BCP) was demonstrated [13]. Metal complexes and polymeric electroactive materials were found to be capable of electroplex formation which were used for the fabrication of white OLEDs [14,15]. However, the number of electroplex-forming molecules is still low which limits diversity of color of electroplex emission and efficiency of electroplex emitters. To better unclose potential of usage of electroplex emitters for OLED applications, the search for new electroplex-forming molecules is still an urgent task.

Phenanthroimidazole–based derivatives called quite big attention of scientific community due to their attractive bipolar properties and excellent luminescence efficiency. Mainly, phenanthroimidazole–based materials were exploited in two application areas related to OLED's relying on their emitting or bipolar properties. Starting with the publication of Wang et al [16]

phenanthroimidazole–based derivatives were developed and used mainly as deep blue singlet emitters for organic light emitting diodes [17], nevertheless some of the compounds showed emissions in UV [18] and red regions of electromagnetic radiation [19].

The aim of this work was synthesis and studies of new solid state emissive bipolar electroactive compounds having electron-accepting phenanthroimidazole moieties and electron-donating carbazolyl or diphenylamino units. We studied new phenanthroimidazole derivatives as blue emitters for non-doped OLEDs. In addition, the electroplex forming properties of such compounds were studied in a host:guest emitting layer with a commercial hole-transporting material 4,4′-cyclohexylidenebis[*N*,*N*-bis(4-methylphenyl)benzenamine] (TAPC). Two most promising phenanthroimidazole-based derivatives were used for the fabrication of white OLEDs based on both fluorescence and either electroplex or exciplex emissions.

2. Experimental methods

2.1 Instrumentation

Nuclear magnetic resonance (^{1}H NMR and ^{13}C NMR) spectra were obtained using a Varian Unity Inova (400 MHz (^{1}H), 101 MHz (^{13}C)). All the data are given as chemical shifts in δ (ppm), multiplicity, integration down-field from $(CH_3)_4Si$. Mass spectra were obtained on a Waters ZQ 2000 (Waters). Infrared (IR) spectra were performed on Perkin Elmer Spectrum BX II FT-IR System, using KBr pellets. Elemental analysis was performed with an Exeter Analytical CE-440 Elemental Analyzer. Differential scanning calorimetry (DSC) measurements were performed on Perkin Elmer DSC 8500 (heating/cooling rate 20 ^{o}C/min). Thermogravimetric analysis (TGA) measurements were performed on a Mettler Toledo TGA/SDTA 851e. Fluorescence emission spectra were recorded with a Perkin Elmer LS 55 spectrometer. Quantum yields in solutions determined using comparative method [20]. The solid-state luminescence quantum yields measured by FLS980 spectrometer (Edinburgh Instruments) using integrating sphere supplied by the spectrometer producer. Absorption spectra were recorded with a Perkin Elmer Lambda 35 spectrophotometer.

Electrochemical investigations carried out using μ-AUTOLAB III (Metrohm Autolab B.V.) potentiostat-galvanostat. The solutions of the synthesized compounds with the concentration of 10^{-3} M were used for cyclic voltamperometry (CV) measurements. The standard ferrocene/ferrocenium redox system used as an internal standard for calculating ionisation potentials [21]. The ionization potentials (I_{PE}) were obtained by the electron photoemission method in air as described earlier [22, 23]. The samples for the measurements were prepared by casting THF solutions of the compounds onto pre-cleaned indium tin oxide (ITO) coated glass substrates. Charge drift mobilities of the vacuum deposited layers of the compounds were tested by the time-of-flight (ToF) method as described earlier [24,25]. Diode-like samples with the thicknesses of layers ranging from 1.8 to 7.1 µm and with bottom ITO and top aluminium electrodes were fabricated. The experimental setup included a Nd:YAG laser EKSPLA NL300, a oscilloscope Tektronix TDS 3032C, and a 6517B Keithley electrometer. To estimate the charge drift mobilities, the formula $\mu=d^2(U\times t_{tr})^{-1}$ was used, where d is the layer thickness, U is applied voltage to the samples, and t_{tr} is the transit time. OLEDs containing non-doped and doped emitting layers with the following architectures were fabricated: ITO/MoO$_3$(3 nm)/m-MTDATA(30 nm)/ the synthetized compound (20 nm)/PBD(10 nm)/TPBi(25 nm)/Ca(10 nm)/Al(60 nm) and ITO/MoO$_3$(3 nm)/m-MTDATA(30 nm)/ the molecular mixture of the synthesized compounds with TAPC or m-MTDATA (20 nm)/PBD(10 nm)/TPBi(25 nm)/Ca(10 nm)/Al(60 nm). The layers of organic compounds and those of calcium and aluminium were prepared by vacuum-deposition under the vacuum of $2\text{-}5\times10^{-6}$ mBar using the equipment from Kurt J. Lesker in-built in an MB EcoVap4G glove box. Before deposition of the layers, the ITO-coated glass substrates with a sheet resistance of 15 Ω/sq were cleaned in acetone and isopropyl alcohol ultrasonic bath during ca. 10 min. To record the density-voltage and luminance-voltage characteristics, a Keithley 6517B electrometer and a Keithley 2400-C source-meter were used in air without passivation immediately after the formation of OLEDs. A calibrated photodiode and an

Avaspec-2048XL spectrometer were utilized for the measurements of brightness and electroluminescence spectra, respectively.

Quantum chemical calculations. The computations were performed in the frame of density functional theory (DFT) [25] employing the B3LYP [27] functional with Gaussian 09 program [28]. The 6-31G(d,p) basis set was utilized for all calculations. The spectroscopic properties of the molecules were calculated by mean of time dependent density functional theory method (TDDFT) [29]. Up to 40 excited states were calculated and the theoretical absorption bands were obtained by considering a band half-width at half-maximum 0.3 eV. The theoretical ionization potentials (IP) were calculated at the B3LYP/6-31G(d,p) level as energy difference between neutral and cation radical species at the neutral state geometry. The intramolecular reorganization energies of holes and electrons for the isolated molecules were calculated according the method described in literature [30].

1.1 **Materials**

9,10-phenanthrenequinone (Aldrich, 80%), trifluoromethanesulfonic acid (Aldrich, 98%), sodium hydrosulfite (Aldrich, 85%), sodium-*tert*-butoxide (Aldrich, 97%), bromine (Aldrich, pure), 9-ethyl-3-carbazole-carboxaldehyde (Aldrich, 98%), 18-crown-6 (Aldrich, 99%), copper (Cu) (Aldrich, 99%), tris(dibenzylideneacetone)dipalladium(0) (Aldrich, 97%), tri-*tert*-butylphosphine (P(*t*-Bu)$_3$) (Aldrich, 1 mol/l), *N*-iodosuccinimide (Fluka, 97%), aniline (Fluka, 98%), ammonium acetate (Reachem, 98%), potassium carbonate (K$_2$CO$_3$) (Reachim, 99 %), bis(4-*tert*-butylphenyl)amine (TCI, 90%) were used as received. 2,7-Diiodophenanthrene-9,10-dione (**1**) and 3,6-dibromophenanthrene-9,10-dione (**2**) were synthesized using procedures described in literature [30,31].

1.2 Synthesis

1.2.1 2-(9-Ethyl-9H-carbazol-3-yl)-5,10-diiodo-1-phenyl-1H-phenanthro[9,10-d]imidazole (3)

To a solution of 2,7-diiodophenanthrene-9,10-dione (1) (0.5 g, 1.09 mmol), 9-ethyl-3-carbazolecarboxaldehyde (0.24 g, 1.09 mmol), ammonium acetate (0.84 g, 10.9 mmol) in glacial acetic acid (5 ml) aniline (0.12 g, 1.3 mmol) was added dropwise. The reaction mixture was stirred at 120 $^{\circ}$C and after 2 h cooled to room temperature. Brown precipitate was filtered, washed with methanol and dried. The crude product was purified by column chromatography (silica gel, 3:1 toluene:hexane) to give a white solid. Yield: 0.2 g (25%). **^{1}H NMR** (400 MHz, d_6-DMSO, δ, ppm): 1.10 (t, *J*=7.0 Hz, **3H**), 4.46 (q, *J*=7.0 Hz, **2H**) 7.21-7.28 (m, **1H**), 7.38 (d, *J*=1.8 Hz, **1H**), 7.46-7.54 (m, **1H**), 7.58-7.68 (m, **2H**), 7.73-7.88 (m, **7H**) 7.97-8.07 (m, **2H**), 8.37 (s, **1H**), 8.65-8.74 (m, **2H**), 9.07 (d, *J*=1.8 Hz, **1H**). **^{13}C NMR** (101 MHz, CDCl$_3$, δ, ppm): 152.34, 140.99, 140.30 (3C), 138.47, 131.86 (2C), 130.39 (2C), 130.16, 129.10 (3C), 127.64, 127.14, 126.88, 126.09, 125.39, 124.58 (2C), 122.89, 122.72, 121.80 (2C), 120.53 (2C), 120.18, 119.37 (2C), 114.07, 108.68, 108.29, 37.66, 13.81. **IR**, KBr, (cm^{-1}): 3057, v (CH$_{ar}$); 2975, v, (CH$_{aliph}$); 1591, v (C=C-N); 1559, 1498, 1453, v (C=C$_{ar}$); 1346, v (C-N); 808, 748, 699, γ (C-H$_{ar}$); 474, v (C-I). **MS** (APCl$^+$, 25 V), m/z: 740 ([M+H]$^+$), (C$_{35}$H$_{23}$I$_2$N$_3$, MW=739.39 g/mol)

1.2.2 6,9-Dibromo-2-(9-ethyl-9H-carbazol-3-yl)-1-phenyl-1H-phenanthro[9,10-d]imidazole (4)

The compound was prepared from 3,6-dibromophenanthrene-9,10-dione (2) (0.5 g, 1.37 mmol), 9-ethyl-3-carbazolecarboxaldehyde (0.3 g, 1.37 mmol), aniline (0.153 g, 1.64 mmol), ammonium acetate (1.05 g, 13.7 mmol), and 5 ml glacial acetic acid using a similar synthesis procedure for **3**, affording a yellow solid. Yield: 0.6 g (68 %). **^{1}H NMR** (400 MHz, d_6-DMSO, δ, ppm.): 1.0 (t, *J*=7.1 Hz, **3H**), 4.44 (q, *J*=7.1 Hz, **2H**), 7.04 (d, *J*=8.9 Hz, **1H**), 7.14-7.28 (m, **1H**), 7.46-7.51 (m, **1H**), 7.56-7.61 (m, **2H**), 7.63 (d, *J*=8.2 Hz, **1H**), 7.69-7.74 (m, **3H**), 7.76-7.80 (m, **2H**), 7.95-8.01 (m, **2H**), 8.29 (d, *J*=1.5 Hz, **1H**), 8.68 (d, *J*=8.6 Hz, **1H**), 9.20 (d, *J*=1.7 Hz, **1H**),

9.22 (d, J=1.9 Hz, 1**H**). **^{13}C NMR** (101 MHz, CDCl$_3$, δ, ppm.): 152.60 (2C), 140.32, 140.14, 138.70 (2C), 130.87, 130.34 (2C), 130.02, 129.90, 129.46, 129.23 (2C), 128.63, 127.69, 127.16, 126.90, 126.05, 125.90, 125.84, 124.75, 122.89, 122.69, 122.27, 121.86, 121.74, 120.46, 119.91, 119.32, 119.04, 108.68, 108.24, 37.65, 13.80. **IR** KBr, (cm^{-1}): 3050, v (CH$_{ar}$); 2968, v, (CH$_{aliph}$); 1598, v (C=C-N); 1508, 1495, 1452, v (C=C$_{ar}$); 1350, v (C-N); 810, 751, 702, γ (C-H$_{ar}$); 539, v (C-Br). **MS** (APCl$^+$, 25 V), m/z: 646 ([M+H]$^+$), (C$_{35}$H$_{23}$Br$_2$N$_3$, MW=645.39 g/mol)

1.2.3 N-(4-(5,10-diiodo-1-phenyl-1H-phenanthro[9,10-d]imidazol-2-yl)phenyl)-N-phenyl-

  *benzenamine (**5**)*

To a solution of 2,7-diiodophenanthrene-9,10-dione (**1**) (0.5 g, 1.09 mmol) in glacial acetic acid (5 ml) 4-(diphenylamino)benzaldehyde (0.3 g, 1.09 mmol), ammonium acetate (0.83 g, 10.9 mmol) and aniline (0.12 g, 1.3 mmol) were added. The temperature was increased to 120 ^{o}C. After 2 h, the reaction mixture was cooled to room temperature. The precipitate was filtered, washed with methanol and dried. The crude product was purified by column chromatography (silica gel, 3:1 toluene:hexane) to give a yellow solid. Yield: 0.6 g (71 %). **^{1}H NMR** (400 MHz, CDCl$_3$, δ, ppm.): 6.94–6.98 (m, **2H**), 7.05–7.12 (m, **9H**), 7.25–7.31 (m, **6H**), 7.37 (d, J = 1.7 Hz, **1H**), 7.45–7.48 (m, **2H**), 7.74 (dd, J = 6.2 Hz, J = 2.6 Hz, **1H**), 7.91 (dd, J = 6.0 Hz, J = 2.0 Hz, **1H**), 8.33 (d, J = 8.9 Hz, **1H**), 8.38 (d, J = 8.9 Hz, **1H**), 9.23 (d, J = 1.9 Hz, **1H**). **^{13}C NMR** (101 MHz, CDCl$_3$, δ, ppm.): 176.60 (2C), 147.07, 134.42 (2C), 133.37, 130.39 (3C), 130.08 (4C), 129.39 (6C), 128.92 (3C), 126.88, 125.39 (2C), 125.19 (6C), 124.58, 123.70 (3C), 121.69 (2C), 93.85, 92.64. **IR**, KBr, (cm^{-1}): 3058, v (CH$_{ar}$); 1610, v (C=C-N); 1592, 1524, 1490, v (C=C$_{ar}$); 1331, v (C-N); 797, 742, 695, γ (C-H$_{ar}$); 436, v (C-I). **MS** (APCl$^+$, 25 V), m/z: 712.21 ([M-C$_6$H$_5$]$^+$), (C$_{39}$H$_{25}$I$_2$N$_3$, MW=789.44 g/mol)

1.2.4 N-(4-(6,9-dibromo-1-phenyl-1H-phenanthro[9,10-d]imidazol-2-yl)phenyl)-N-

phenylbenzenamine (6)

The compound was prepared from 3,6-dibromophenanthrene-9,10-dione (**2**) (0.5 g, 1.37 mmol), 4-(diphenylamino)benzaldehyde (0.37 g, 1.37 mmol), aniline (0.15 g, 1.65 mmol), ammonium acetate (1.05 g, 13.7 mmol), and 5 ml of glacial acetic acid using a similar synthesis procedure for **5**, yellow crystals was finally obtained. Yield: 0.5 g (53 %). **^{1}H NMR** (400 MHz, d_6-DMSO, δ, ppm.): 7.08–7.17 (m, **11H**), 7.33–7.41 (m, **6H**), 7.90 (d, *J*=8.5 Hz, **2H**), 8.15 (d, *J*=8.8 Hz, **2H**), 8.46 (d, *J* = 8.6 Hz, **2H**), 9.11 (d, *J*=1.4 Hz, **2H**). **^{13}C NMR** (101 MHz, d_6-DMSO, δ, ppm.): 150.38, 148.87, 147.17 (2C), 131.04 (2C), 130.22 (7C), 128.59, 127.95 (2C), 127.27 (2C), 125.21 (7C), 124.30 (6C), 123.93, 122.50 (2C), 119.20 (2C). **IR** KBr, (cm^{-1}): 3035, v (CH$_{ar}$); 1612, v (C=C-N); 1591, 1519, 1477, v (C=C$_{ar}$); 1331, v (C-N); 812, 738, 695, γ (C-H$_{ar}$); 542, v (C-Br). **MS** (APCl$^+$, 25 V), m/z: 618.03([M-C$_6$H$_5$]$^+$), (C$_{39}$H$_{25}$Br$_2$N$_3$, MW=695.44 g/mol)

1.2.5 5,10-Bis(3,6-di-tert-butyl-9H-carbazol-9-yl)-2-(9-ethyl-9H-carbazol-3-yl)-1-phenyl-1H-

phenanthro[9,10-d]imidazole (7).

To a solution of 2-(9-ethyl-9H-carbazol-3-yl)-5,10-diiodo-1-phenyl-1*H*-phenanthro[9,10-d]imidazole (**3**) (0.05 g, 0.07 mmol), 3,6-di-*tert*-butylcarbazole (0.06 g, 0.21 mmol) and 18-crown-6 (0.004 g, 0.014 mmol) in *o*-dichlorobenzene (1 ml) were added K$_2$CO$_3$ (0.027 g, 0.21 mmol) and Cu powder (0.018 g, 0.28 mmol). The reaction was stirred at 190 ^{o}C for 24 h under argon atmosphere. Insoluble inorganic salts were removed by filtration and washed with small amount of toluene. After removal of *o*-dichlorobenzene brown liquid was added to hexane. The precipitate was collected by filtration and purified by column chromatography (silica gel, 6:1 hexane:acetone) to give a white solid. Yield: 0.05 g (70 %). **^{1}H NMR** (400 MHz, CDCl$_3$, δ, ppm.): 1.42 (t, *J*=7.0 Hz, **3H**), 1.54 (d, *J*=3,9 Hz, **36H**), 4.34 (q, *J*=7.0 Hz, **2H**), 7.16-7.69 (m, **17H**), 7.80-7.95 (m, **5H**), 8.15 (s, **1H**), 8.25 (s, **3H**), 8.97 (d, *J*=8.9 Hz, **1H**), 9.03 (d, *J*=9,0 Hz, **1H**), 7.56-7.64 (m, **2H**), 9.23 (d, *J*=1.7 Hz, **1H**). **^{13}C NMR** (101 MHz, CDCl$_3$, δ, ppm.*)*: 152.77, 143.32, 142.97 (2C), 140.30,

140.03, 139.52, 138.90, 138.55 (2C), 137.97, 137.28, 136.28, 130.55 (3C), 129.77, 128.90 (2C), 128.45, 127.24, 126.88, 126.59, 125.84 (3C), 124.94, 124.29, 124.09, 123.59 (8C), 122.95, 122.64, 121.61, 120.39 (4C), 119.23 (2C), 117.69, 116.12 (3C), 109.62 (4C), 108.61 (2C), 108.27, 34.80 (2C), 32.07 (16C). **IR**, KBr, (cm^{-1}): 3045, v (CH$_{ar}$); 2959, v, (CH$_{aliph}$); 1614, v (C=C-N); 1531, 1479, 1452, v (C=C$_{ar}$); 1349, v (C-N); 810, 749, 703, γ (C-H$_{ar}$). **MS** (APCl^{+}, 25 V), m/z: 1042.6 ([M]$^{+}$), (C$_{75}$H$_{71}$N$_5$, MW=1042.4 g/mol). **Anal. Calcd**. for C$_{75}$H$_{71}$N$_5$: C, 86.42; H, 6.87; N, 6.71 %; found C 86.37, H 6.90, N 6.73%.

1.2.6 6,9-Bis(3,6-di-tert-butyl-9H-carbazol-9-yl)-2-(9-ethyl-9H-carbazol-3-yl)-1-phenyl-1H-phenanthro[9,10-d]imidazole (8)

To a solution of 6,9-dibromo-2-(9-ethyl-9*H*-carbazol-3-yl)-1-phenyl-1*H*-phenanthro[9,10-d]imidazole (**4**) (0.2 g, 0.31 mmol), 3,6-di-*tert*-butylcarbazole (0.2 g, 0.71 mmol) and *t*-BuONa (0.18 g, 1.86 mmol) in anhydrous toluene (5 ml) were added Pd$_2$(dba)$_3$ (0.012 g, 0.01 mmol) and P(*t*-Bu)$_3$ (0.003 g, 0.001 mmol, 0,1 M solution in toluene). The reaction was stirred at 110 ^{o}C for 24 h under argon atmosphere. Solvent was removed using vacuum, the precipitate was purified by column chromatography (silica gel, toluene) to give a yellow solid. Yield: 0.11 g (34 %). **¹H NMR** (400 MHz, d$_6$-DMSO, δ, ppm.): 1.31 (t, *J*=7.0 Hz, **3H**), 1.39 (d, *J*=5.7 Hz, **36H**), 4.46 (q, *J*=6.9 Hz, **2H**), 7.21-7.29 (m, **2H**), 7.38 (d, *J*=8.7 Hz, **1H**), 7.34-7.54 (m, **6H**), 7.58-7.68 (m, **3H**), 7.73-7.79 (m, **3H**), 7.81 (dd, *J*=8.6 Hz, *J*=1.7 Hz, **1H**), 7.88-7.93 (m, **2H**), 8.03 (d, *J*=7.5 Hz, **2H**), 8.26 (d, *J*=1.7 Hz, **1H**), 8.31 (d, *J*=1.6 Hz, **1H**), 8.37 (d, *J*=1.5 Hz, **1H**), 9.03 (d, *J*=8.5 Hz, 1**H**), 9.25 (s, 1**H**), 9.29 (s, 1**H**). **¹³C NMR** (101 MHz, d$_6$-DMSO, δ, ppm.): 153.04, 149.48, 147.51, 142.95, 139.12, 138.14, 137.32, 136.36, 135.43, 134.78, 133.68, 130.03 (2C), 129.93 (2C), 129.40, 127.66 (2C), 125.80 (2C), 125.75, 125.67 (2C), 125.22, 124.36, 124.33 (2C), 123.27 (2C), 123.09, 122.22 (2C), 121.56, 121.46, 121.30, 121.16, 120.94, 120.01 (2C), 119.35 (2C), 118.75, 117.78, 117.20 (2C), 116.26, 113.63, 113.45, 109.62 (3C), 109.34 (2C), 109.20, 106.69 (3C), 34.97 (2C), 32.30 (16C). **IR**, KBr, (cm^{-1}): 3053, v (CH$_{ar}$); 2954, v, (CH$_{aliph}$); 1616, v (C=C-N); 1489, 1475, 1457, v

(C=C$_{ar}$); 1348, v (C-N); 809, 746, 702, γ (C-H$_{ar}$). **MS** (APCl$^+$, 25 V), m/z: 1042.6 ([M]$^+$), (C$_{75}$H$_{71}$N$_5$, MW=1042.4 g/mol). **Anal. Calcd**. for C$_{75}$H$_{71}$N$_5$: C, 86.42; H, 6.87; N, 6.71 %; found C 86.39, H 6.89, N 6.72%.

*1.2.7 2-(4-(Diphenylamino)phenyl)-5,10-(4-tert-butylphenyl)-1-phenyl-1H-phenanthro[9,10-d]imidazole-5,10-diamine (**9**)*

The compound was prepared from *N*-(4-(5,10-diiodo-1-phenyl-1*H*-phenanthro[9,10-d]imidazol-2-yl)phenyl)-*N*-phenyl-benzenamine (**5**) (0.5 g, 0.6 mmol), bis(4-*tert*-butylphenyl)amine (0.51 g, 1.8 mmol), 18-crown-6 (0.032 g, 0.12 mmol), K$_2$CO$_3$ (0.23 g, 1.8 mmol), copper powder (0.15 g, 2.4 mmol), and 6 ml of *o*-dichlorobenzene using a similar synthetic procedure as for compound **7**, white solid was finally obtained. Yield: 0.1 g (15 %). **^{1}H NMR** (400 MHz, CDCl$_3$, δ, ppm.): 1.34-1.39 (m, **36H**), 6.85-6.90 (m, **8H**), 7.00-7.07 (m, **14H**), 7.12-7.17 (m, **3H**), 7.20-7.27 (m, **14H**), 7.32-7.37 (m, **2H**). **^{13}C NMR** (101 MHz, CDCl$_3$, δ, ppm.): 145.35 (14C), 129.80 (3C), 129.29 (6C), 128.49 (4C), 125.89 (9C), 125.00 (8C), 123.61 (19C), 31.52 (16C). **IR**, KBr, (cm^{-1}): 3060, v (CH$_{ar}$); 2960, v, (CH$_{aliph}$); 1599, v (C=C-N); 1510, 1460, v (C=C$_{ar}$); 1317, v (C-N); 807, 754, 695, γ (C-H$_{ar}$). **MS** (APCl$^+$, 25 V), m/z: 1096.9 ([M]$^+$), (C$_{79}$H$_{77}$N$_5$, MW=1096.5 g/mol). **Anal. Calcd**. for C$_{79}$H$_{77}$N$_5$: C, 86.53; H, 7.08; N, 6.39 %; found C 86.48, H 7.11, N 6.41%.

*1.2.8 2-(4-(Diphenylamino)phenyl)-6,9-(4-tert-butylphenyl)-1-phenyl-1H-phenanthro[9,10-d]imidazole-6,9-diamine (**10**).*

The compound was prepared from *N*-(4-(6,9-dibromo-1-phenyl-1*H*-phenanthro[9,10-d]imidazol-2-yl)phenyl)-*N*-phenylbenzenamine (**6**) (0.4 g, 0.58 mmol), bis(4-*tert*-butylphenyl)amine (0.37 g, 1.33 mmol), *t*-BuONa (0.33 g, 3.48 mmol), Pd$_2$(dba)$_3$ (0.024 g, 0.02 mmol), P(*t*-Bu)$_3$ (0.006 g, 0.002 mmol, 0,1 M solution in toluene), and 5 ml of anhydrous toluene using a similar synthetic procedure as for **8**, affording a white solid. Yield: 0.35 g (56 %). **^{1}H NMR** (400 MHz, d$_6$-DMSO, δ, ppm.): 2.09 (m, **36H**), 7.11-7.21 (m, **25H**), 7.22-7.30 (m, **16H**). **^{13}C NMR**

(101 MHz, CDCl$_3$, δ, ppm.): 144.57 (6C), 130.19 (9C), 129.26 (14C), 128.15 (3C), 125.65 (25C), 123.51 (6C), 31.47 (16C). **IR**, KBr, (cm^{-1}): 3034, v (CH$_{ar}$); 2958, v, (CH$_{aliph}$); 1591, v (C=C-N); 1510, 1473, v (C=C$_{ar}$); 1317, v (C-N); 828, 753, 695, γ (C-H$_{ar}$). **MS** (APCl$^+$, 25 V), m/z: 1096.64 ([M]$^+$), (C$_{79}$H$_{77}$N$_5$, MW=1096.5 g/mol). **Anal. Calcd**. for C$_{79}$H$_{77}$N$_5$: C, 86.53; H, 7.08; N, 6.39 %; found C 86.50, H 7.12, N 6.38%.

3. Results and Discussion

Synthetic routes for the donor-substituted phenanthroimidazole derivatives **7**-**10** are outlined in **Scheme 1**. The starting compounds **1** and **2** were prepared according to the procedures earlier reported in literature [31,32]. The key intermediate phenanthroimidazole derivatives **3-6** were obtained by the reactions of compounds **1** or **2** with the corresponding aldehydes. The target compounds **7** and **9** were prepared by Ullmann coupling reactions [33]. Derivatives **8** and **10** were synthesized using Buchwald-Hartwig conditions [34]. All the synthesized compounds were purified by column chromatography and characterized by IR, NMR spectroscopies and mass spectrometry, elemental analyses as described in the experimental section.
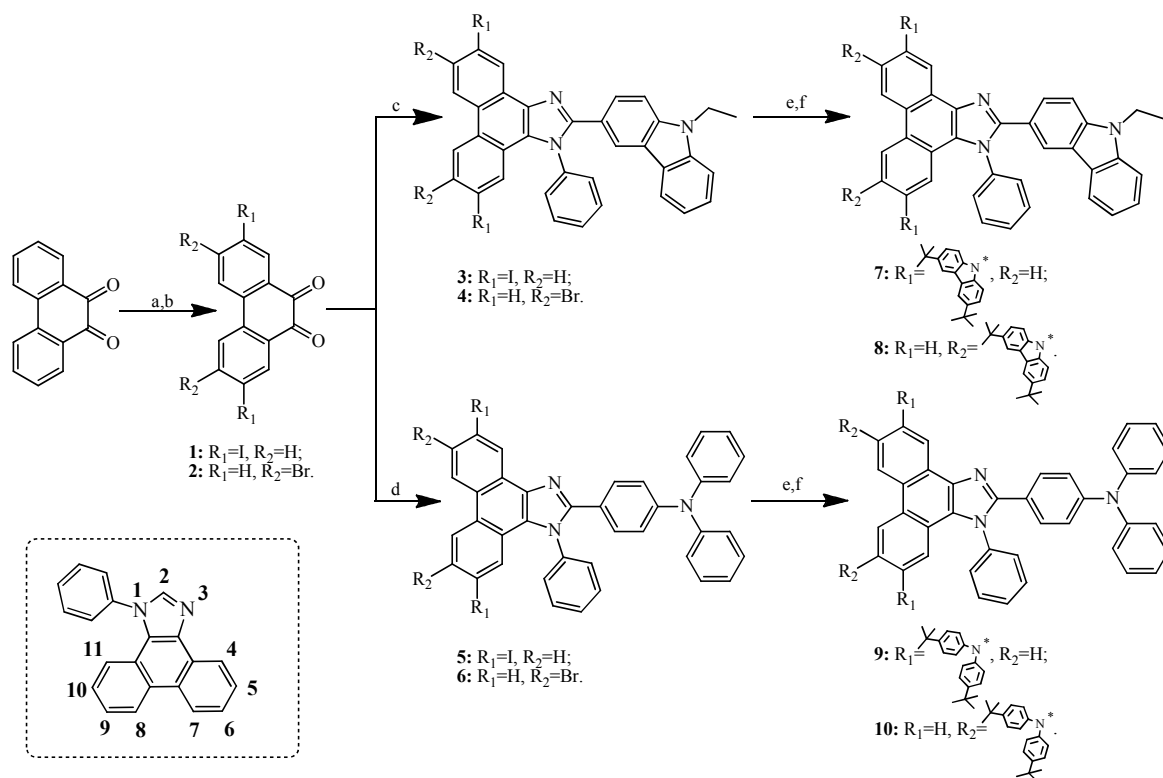
Scheme 1. Synthetic routes for phenanthroimidazole derivatives. **a.** *N*-iodosuccinimide, CF$_3$SO$_3$H, 6 h, 20 ^{o}C; **b.** Br$_2$, NaHSO$_3$, nitrobenzene, 22 h, 120 ^{o}C; **c.** 9-ethyl-3-carbazolecarboxaldehyde, CH$_3$CO$_2$NH$_4$, aniline, CH$_3$COOH, 2h, 120 ^{o}C; **d.** 4-(diphenylamino)benzaldehyde, ammonium acetate, aniline, CH$_3$COOH, 2h, 120 ^{o}C; **e.** 3,6-di-*tert*-butylcarbazole (bis(4-tert-butylphenyl)amine), 18-crown-6, Cu, K$_2$CO$_3$, *o*-dichlorobenzene, 24h (48h), 190 ^{o}C; **f.** 3,6-di-*tert*-butylcarbazole (bis(4-*tert*-butylphenyl)amine), *t*-BuONa, Pd$_2$(dba)$_3$, P(*t*-Bu)$_3$, toluene, 24 h, 110 ^{o}C.

3.1 Thermal properties

The thermal properties of phenanthroimidazole derivatives **7-10** were investigated by TGA and DSC under a nitrogen atmosphere. Their thermal characteristics are summarized in **Table 1**. All compounds exhibit high thermal stability and glass-forming ability. Their 5% weight-loss temperatures (T$_d$) range from 491 to 524 °C. The DSC curves of the second heating of the compounds **7-10** demonstrate that compounds could be transformed into amorphous state (**Figure 1**). The glass-transition temperatures (T$_g$) of **7-10** were observed in the range of 183-239 ^{o}C. Compounds **7** and **8** containing carbazole moieties exhibited considerably higher T$_g$ than phenanthroimidazole derivatives **9** and **10** containing diphenylamino substituents. This observation

13

can apparently be explained by the higher rigidity of carbazole moiety. Such high T_g and T_d values of compounds **7-10** indicate that the amorphous layers of these compounds can be fabricated by vacuum thermal evaporation technology. In addition, materials are expected to exhibit high morphological stability which is desirable for the materials used in OLEDs [35].

Table 1. Thermal characteristics of compounds **7-10**

Compound	T_m^a (°C)	T_g^a (°C)	T_d^b (°C)
7	-	206	524
8	-	239	511
9	394	192	491
10	-	183	503

[a] Determined by DSC, scan rate 20 °C/min, N_2 atmosphere. [b] T_d is 5% weight loss temperature; scan rate 20 °C/min, N_2 atmosphere.
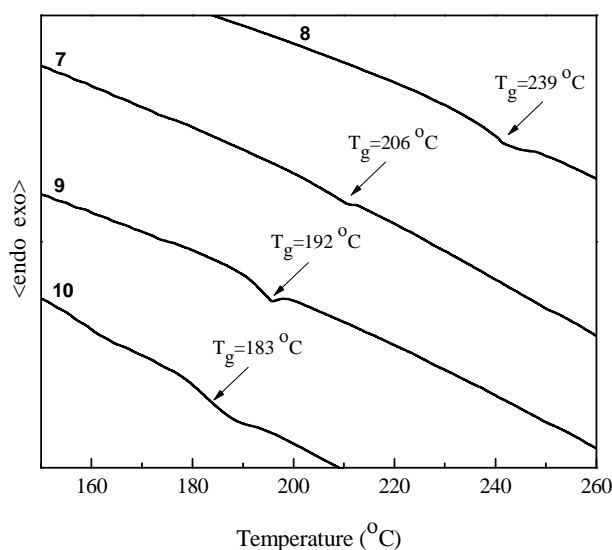

Figure 1. DSC curves (2nd heating) of the phenanthroimidazole derivatives **7-10**, at the heating rate of 20 °C/min, N_2 atmosphere

3.2 Geometries and frontier orbitals

The theoretical geometries of synthesized compounds **7**-**10** are presented in **Figure 2**. The fused phenanthroimidazole core is planar and substituents attached to it are out of plane with dihedral angles in the range of 22-76°. In the case of **7** and **8**, the dihedral angles between carbazole moieties with *tert*-butyl groups and phenyl rings of central plane are ranging from 51° to 58°. The replacement of carbazole substituents by diphenylamino moieties in **9** and **10** leads to decreased dihedral angles (38°- 49°). It was found, that substituents at 10th position of phenanthroimidazole are weakly affected by phenyl ring attached at imidazolyl moiety. Therefore, carbazole and diphenylamine at this position are more twisted than their analogues fragments attached at 5th position (7° for **7** and 11° for **9**).
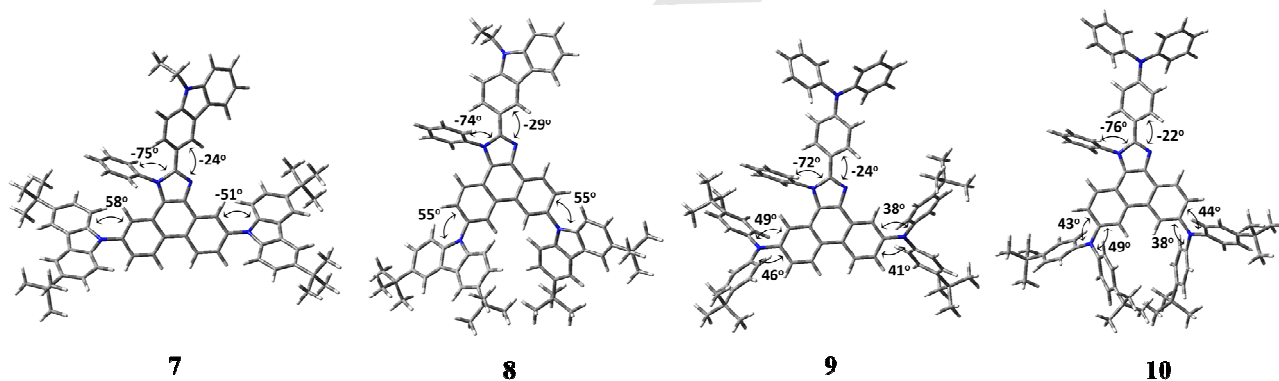

Figure 2. Optimized geometries of compounds **7**-**10** obtained at B3LYP/6-31G(d, p) level

The HOMO for the molecules with substituents at the same positions were found to be very similar (**Figure 3**). In the case of **7** and **9**, HOMO is localized on phenyl rings of the central core and substituents with *tert*-butyl groups. However, due to the larger inter-fragment dihedral angles in compound **7** as compared to **9** by roughly 10 ° (**Figure 2**), the bridging between the two lateral substituents through the core is less efficient in the case of compound **7** (**Figure 3**). The above explanation is also consistent with the larger contributions in the HOMO of compounds **7** and **9** from the substituents at 5th position (dihedral angles of 38-41° and 51° respectively) as compared to those at 10th position (dihedral angles of 46-49° and 58°). In the case of compounds **8** and **10**,

15

HOMO is essentially distributed over the entire phenanthroimidazole core, with less contribution from the 9-ethylcarbazole or triphenylamine units.

The LUMOs of compounds **7**-**10** are mainly localized on the central core, exhibiting some additional distribution on the substituents attached to the imidazole ring (**Figure 3**), in turn being more important in the case of triphenylamine substituents (compounds **9** and **10**). The energies of the frontier orbitals (**Figure** 3, **Table S1**) translate the above observations, indicating higher HOMO energies for **9** and **10** due to better conjugation between the central core and the substituents. The range of the LUMO energies is narrower, which is due to enhanced LUMO similarity across the series as compared to HOMOs.
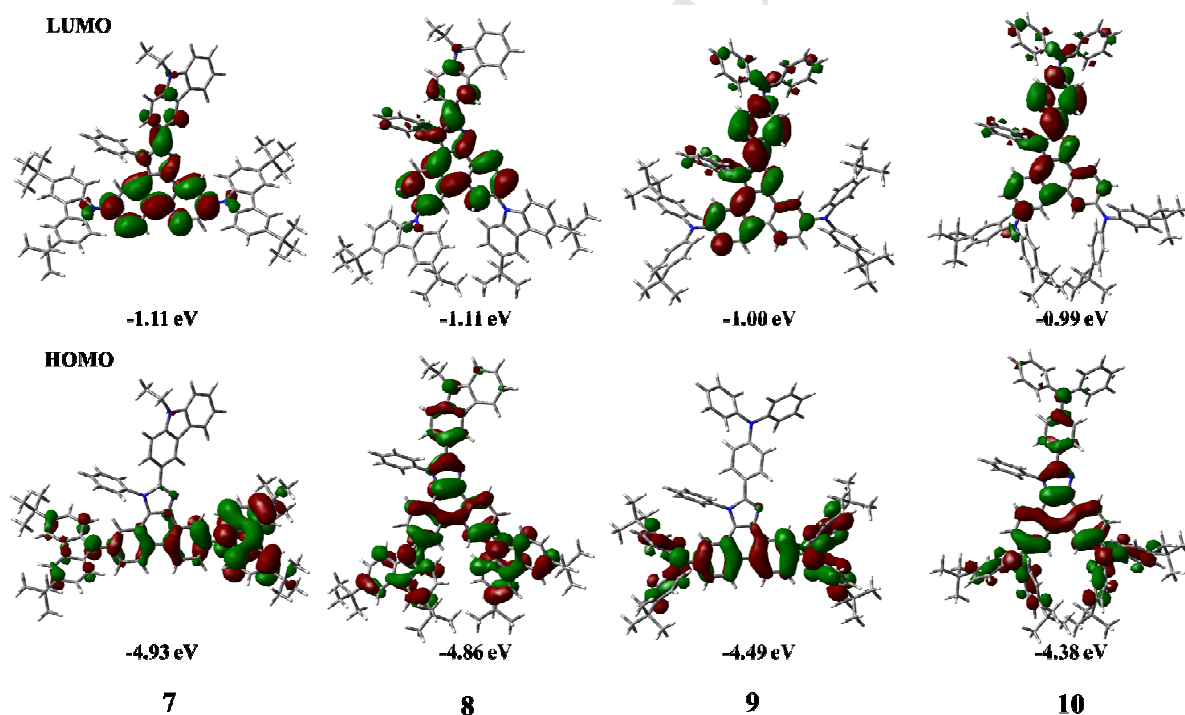

Figure 3. HOMO and LUMO of compounds **7**-**10** calculated at B3LYP/6-31G(d,p) level

3.3 Optical and photophysical properties

The experimental absorption spectra of the dilute solutions of **7-10** in tetrahydrofuran (THF) are in agreement with the theoretical spectra (**Figure 4**). The optical characteristics are summarized in **Table 2** and **Table S1**. The lowest energy absorption bands of compounds with diphenylamino

moieties (**9** and **10)** are red-shifted with respect to those of phenanthroimidazole derivatives **7** and **8** containing carbazole substituents. This is due to more effective conjugation of π-electrons in **9** and **10** molecules over all π-backbone (**Figure 3**) which lead to the smaller values of band gap for those compounds. The band gaps decrease in the order **7** > **8** > **9** > **10** (3.82 eV > 3.75 eV > 3.49 eV > 3.39 eV). According to the results of quantum chemical calculations, the lowest energy absorption bands of derivatives **7-10** can be characterized as a mixture of electronic transitions towards several excited states (**Figure S1**). The transition from ground state to first excited state ($S_0 \rightarrow S_1$) in compounds **7-10** correspond to transition from HOMO to LUMO, LUMO+1. Absorption spectra of the films of compounds **7-10** are similar to those of dilute solutions (**Figure S2**). The lowest energy absorption bands of the films of compound **7-9** are slightly red-shifted with respect of those of the solutions, due to enhanced intermolecular interactions in the solid state, whereas no shift is observed in the case of compound **10**. The HOMO distributions (**Figure 3**) indeed indicate larger contribution of the peripheral molecular entities in the case of compounds **7-9**, hence larger sensitivity of HOMO energies to intermolecular interactions and geometrical deformations, as compared to compound **10**.
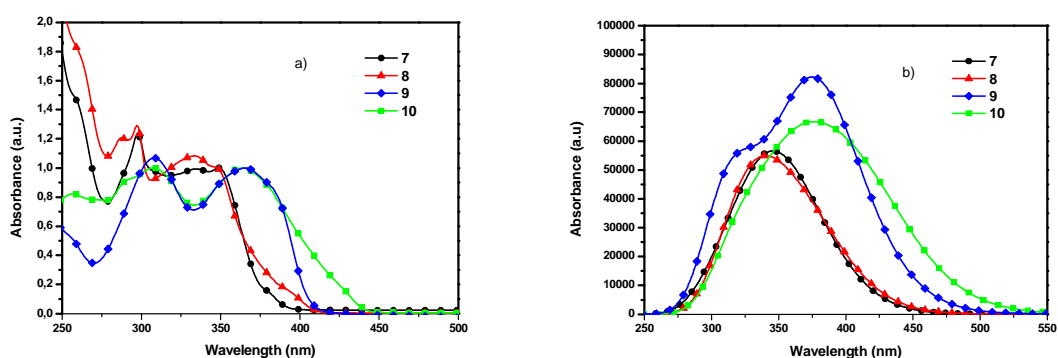

Figure 4. Normalized experimental (a) and theoretical in gas phase (b) absorption spectra of compounds **7**-**10**

Fluorescence and phosphorescence spectra and photophysical properties of the dilute solutions of **7-10** in THF are presented in **Figure 5** and **Table 2**. The spectra of the solutions of compounds exhibit emission peaks in the range from 414 to 467 nm. In the solid state, the emission

17

of these four materials show negligible red shift with emission intensity maxima still localized in the blue spectral region (421 - 468 nm) (**Figure S2**), which is coherent with the similar red-shifts of the corresponding absorption spectra. Fluorescence spectra presented in **Figure 5** translate consequently the effective conjugation of π-electrons over all π-backbone (or the substituent-core π-donor efficiency) in the molecules as it was mentioned previosly. The similar observations were recently reported for triazol-containing derivatives [36,37]. In the case of carbazolyl substituted compounds (**7**, **8**) for instance, the emission maxima are blue-shifted compared to the spectra of the derivatives containing diphenylamino moieties (**9**, **10**), which is coherent with the same trend observed for the low energy absorption bands and the theoretical results (**Figure 3** and **Table 2**). On the other hand, the position of emission bands also depends on substitution pattern of phenanthroimidazole chromophore. The emission is blue-shifted in the case of phenanthroimidazole moiety substituted at 5th and 10th positions (**7**, **9**) compared to the spectra of the derivatives having substituents at 6th and 9th positions (**8**, **10**), in agreement with the smaller degree of HOMO delocalizations in compounds **7**, **9** as compared to **8** and **10**. Both the nature of the substituent and the linking position are important for tuning the emission colour of the synthesised phenanthroimidazoles.

Fluorescence quantum yields (Φ_f) of the solid films of compounds **7-9** were found to be considerably higher than those of dilute THF solutions and reach 0.55 (**Table 2**). Quantum chemical calculations revealed that optimized geometries show quite large dihedral angles between phenanthroimidazole moiety and bulky donors - *tert*-butylated carbazolyl and diphenylamino units. The increase of the Φ_f values in solid state could be due to freezing of rotational degrees of freedom between the substituents and the phenanthroimidazole core in the case of compounds **7-9**, thus suggesting an effect similar to aggregation induced enhanced emission (AIEE) [38]. This hypothesis seems to be supported by the coherence between the geometrical characteristics of the compounds and their Φ_f. Indeed, in the case of compounds **7** and **9**, the phenyl group of the

18

imidazole ring prevents from rotations of neighbour substituents in 10th position, whereas the rotations of the substituents in 5th position are free from steric hindrance. The corresponding contribution to the self-quenching in solution can thus be reduced (eliminated) in solid films, resulting in increased Φ_f. In the case of compound **8** both groups in 6th and 9th positions seem to undergo free rotations in solution (no steric hindrance from the phenyl ring), hence resulting in almost total fluorescence self-quenching (0.09 in THF, **Table 2**). Obviously, this effect is absent in the case of compound **10** (no AEIEE effect, **Table 2**), due to the larger volume of diphenylamino groups as compared to carbazoles, mutually preventing from their free rotations. Indeed, **Figure 2** indicates larger space separation between the two substituents in 6th and 9th positions in compound **8** as compared to **10**.

Commission Internationale de l'Eclairage (CIE) chromaticity coordinates (x,y) for the solution of compounds **7**, **8**, **9**, and **10** were calculated from emission spectra and were found to be (0.16, 0.03), (0.15, 0.03), (0.15, 0.09), and (0.14, 0.07) respectively, which correspond to the blue colour. The lowest energy phosphorescence peaks of **7-10** were observed in the range from 471 to 535 nm. Based on these values the calculated triplet energies of **7**, **8**, **9**, and **10** arrange in the order 2.63 eV > 2.53 eV > 2.46 eV > 2.32 eV, respectively. In the all cases, experimental triplet energies compare well with theoretical vertical values (**Table 2**).

Table 2. Optical and photophysical characteristics of compounds **7-10**

Compound	λ_{abs}(soln/film)[a] (nm)	λ_{FL}(soln/film)[a] (nm)	Φ_f(soln/film)[b]	CIE[c] (x;y)	λ_{Ph}[d] (nm)	E_T(exp/theor)[e] (eV)
7	349/353	414/421	0.35/0.55	(0.16;0.03)	471	2.63/2.65
8	348/350	417;434/424;444	0.09/0.49	(0.15;0.03)	491	2.53/2.61
9	365/374	435/443	0.22/0.51	(0.15;0.09)	505	2.46/2.48
10	364/364	444;467/443;468	0.26/0.27	(0.14;0.07)	535	2.32/2.39

[a] Maxima bands of absorption and fluorescence recorded at room temperature. [b] The fluorescence quantum yield of the solution using a 0.5 M H_2SO_4 solution of quinine as reference (0.51); the solid state quantum yield estimated using an integrating sphere. [c] Estimated from the fluorescence spectra

of the solutions in THF. [d] Lowest energy maxima bands of phosphorescence measured in THF at 77 K. [e] Experimental and theoretical vertical values of triplet energy.
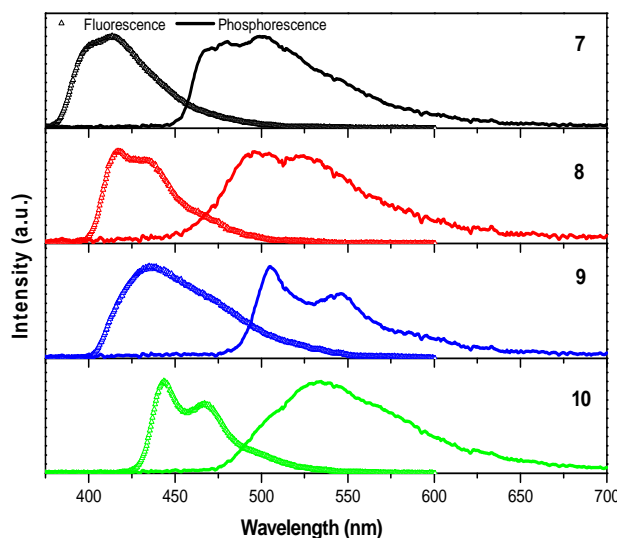

Figure 5. Normalized room temperature fluorescence and phosphorescence recorded at 77K spectra of dilute solutions of **7-10** in THF (10^{-5}).

3.4 Electrochemical and photoelectrical properties

To evaluate applicability of the materials in optoelectronic devices, the electrochemical properties of compounds **7-10** were further studied by CV measurements using their in 10^{-3} M solutions. The results of the CV measurements are shown in **Table 3**. The CV voltamperogram of **10** is given in **Figure 6**. During the positive potential sweep compound **10** showed three reversible oxidation peaks located at 0.42, 0.65 and 1.06 V which indicate the generation of a stable tricationic species. The three-electron process probably could be assigned to the formation of cations on each diphenylamino and triphenylamino moieties.

The other compounds under investigation showed similar behaviour in CV experiments (see **Figure S11**). Has been noticed, that the same values of electrochemical peaks were observed for derivatives **7-10** after repeated cycles. Compounds form stable cations, because active *para* positions of diphenylamino and 3rd, 6th positions of carbazolyl moieties are blocked by *tert*-butyl

20

groups. Additionally, the *para* positions of fragments attached to the imidazole ring lack of HOMO electron density (**Figure 3**).

The ionization potential (IP$_{CV}$) and electron affinity (EA$_{CV}$) values of the compounds were calculated from their onset potentials of oxidation and their $E_{opt}{}^g$. IP$_{CV}$ values of the four compounds varied in the range from 4.96 to 5.52 eV and EA$_{CV}$ values ranged from 2.01 to 2.38 eV. IP$_{CV}$, calculated theoretical IP and HOMO energies have the same trend and decrease in the order **7** > **8** > **9** > **10**. This trend could be explained by chromophore's nature and substitution pattern of phenanthroimidazole moiety. Derivative **7** with carbazolyl units attached at 5th and 10th positions of phenanthroimidazole moiety shows the highest IP and on the contrary the lowest IP was observed for the derivative **10** which contains diphenylamino units attached at 6th and 9th positions of phenanthroimidazole moiety. The difference between ionization potential values estimated by electron photoemission in air method (IP$_{EP}$) and IP$_{CV}$ is due to the different environments in solutions and solid layers of compounds.
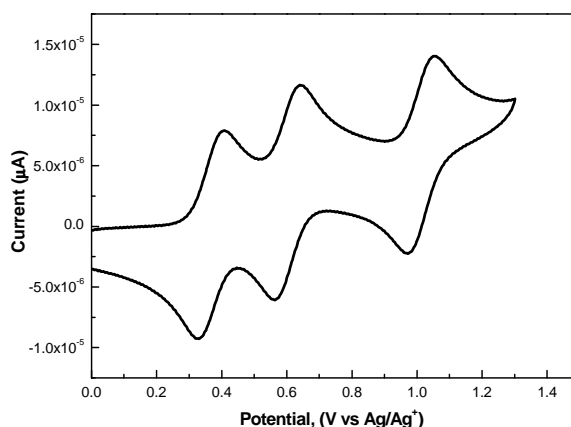

Figure 6. CV of compound **10** (scan rate of 50 mV s^{-1} vs Ag/Ag$^+$).

Table 3. Electrochemical characteristics of compounds **7**-**10**.

Compound	$E_{ox}{}^a$ (V)	$IP_{CV}{}^b$ (eV)	$E_{opt}{}^{g\ c}$ (eV)	$EA_{CV}{}^d$ (eV)	$IP_{EP}{}^e$ (eV)	IP^f, eV
7	1.02	5.52	3.14	2.38	5.29	5.74
8	0.85	5.38	3.04	2.34	5.31	5.61

| **9** | 0.51 | 5.03 | 3.02 | 2.01 | 5.27 | 5.26 |
| **10** | 0.42 | 4.96 | 2.81 | 2.15 | 5.15 | 5.10 |

[a] Onset oxidation potential *vs* Ag/Ag$^+$. [b] $IP_{CV} = (E_{ox} - E_{Fc/Fc}^+) + 4.8$ (eV). [c] Estimated from the onset wavelength of optical absorption according to the empirical formula: $E_{opt}^g = 1240/\lambda_{edge}$, in which the edge is the onset value of absorption spectrum in long wave direction. [d] $EA_{CV} = IP_{CV} - E_{opt}^g$. [e] Established from electron photoemission in air spectra. [f] Theoretical adiabatic IP values.

To examine the charge-transporting properties of compounds **7-10**, the charge-drift mobilities were measured by the ToF technique (**Figure 7, Figure 8, Table 4**). The transit times (t_{tr}) for both holes and electrons on transient curves in log-log scales were well seen showing the ambipolar charge transport for the layers of all the compounds studied (**Figure 8a, b**, **Figure S1**). Hole (μ_h) and electron (μ_e) mobilities for the layers of **7-10** were estimated using the formula $\mu = d^2/(U \times t_{tr})$, where d is the thickness of the layer and U is voltage. Well balanced hole and electron transport was observed for the layers of **7-10**. The vales of μ_e were only slight higher than the values of μ_h (**Figure 7**). Both μ_h and μ_e for the layers of **7-10** confirm Poole–Frenkel type electric field dependence $\mu = \mu_0 \times \exp(\alpha E)^{1/2}$, where μ_0 is the zero electric field charge mobility, and α is the field dependence parameter [39]. This dependence is typically confirmed by organic ambipolar semiconductors (**Figure 7**, **Table 4**) [40]. Close values of charge mobilities in the range from ca. 10^{-5} to 10^{-3} cm^2/(Vs) at electric fields of $(0.4-8.1) \times 10^5$ V/cm were found for compounds **7-10**. The differences in shapes of the current transients for holes and electrons for **7-10** were observed indicating that the hole transport is less dispersive than that of electrons (**Figure 8, Figure S3**).
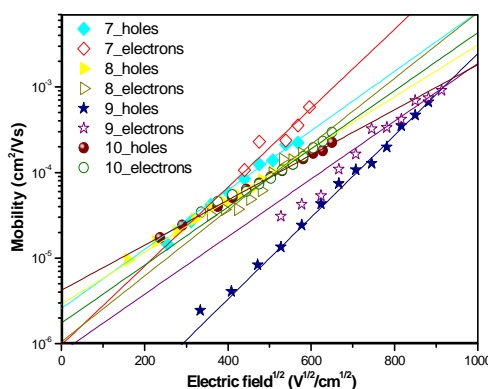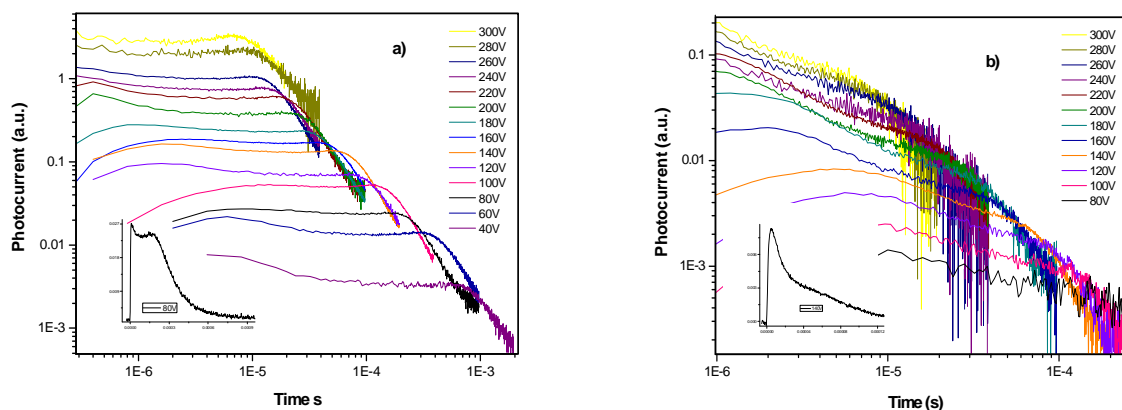
Figure 7. Hole-drift and electron-drift mobilities for the layers of compounds **7-10** at room temperature

Figure 8. Hole (a) and electron (b) transient curves at the different electric fields for **10** and electric field dependencies

To get insight into the charge mobilities in the layers of synthesized compounds, intramolecular reorganization energies of holes (λ_h) and electrons (λ_e) for the isolated molecules of **7-10** were calculated. According Marcus theory [41,42,43], the smaller values of intramolecular reorganization energies will enhance charge mobilities. The λ_h and λ_e values are presented in the **Table 4** and are estimated to increase in the order **7 < 8 ≈ 9 < 10** and **7 < 8 < 9 < 10**, respectively. These values are consistent with the increase of charge mobilities in the order **7 > 8 > 10**, at an electric field of 3.6×10^5 cm^2/Vs (**Table 4**). However, the much larger λ_e values as compared to λ_h ones are inconsistent with the roughly similar (even slightly larger) electron mobilities as compared to hole ones. Additionally, the trend of λ_e values is opposite to the trend of μ_e. These observations indicate that the hole and electron transport in these compounds are dominated by disorder phenomena. Support to this conclusion seems to come from the comparison between HOMO-versus LUMO distributions: LUMOs are more concentrated on the rigid phenanthroimidazole core preventing from large distribution of LUMO energies (density of states). An opposite situation occurs for the HOMO energies, being more sensitive to the deformation of the phenanthroimidazole-ligand dihedral angles.

23

Table 4. Charge-drift mobilities and reorganization energies of compounds **7**-**10**.

Compound	d (μm)	μ_h (cm^2/V·s)^a	λ_h (eV)	μ_e, (cm^2/V·s)^a	λ_e (eV)
7	3.1	3.14×10^{-4}	0.12	5.69×10^{-4}	0.30
8	3.9	1.91×10^{-4}	0.21	2.14×10^{-4}	0.36
9	1.8	3.02×10^{-5}	0.21	8.52×10^{-5}	0.50
10	7.1	1.60×10^{-4}	0.28	1.91×10^{-4}	0.52

^{a} Hole- and electron-drift mobilities at an electric field of $3.6 \cdot 10^5$ cm^2/Vs.

3.5 Electroluminescent properties

Since derivatives **7-10** showed strongly enhanced blue emission in the solid state (Φ_f=0.27-0.55) and ambipolar charge transport with well-balanced hole and electron mobilities, it was of interest to study their electroluminescent properties. Electroluminescent devices based on non-doped light-emitting layers **7-10** with the following architectures were fabricated: ITO/MoO$_3$(3 nm)/m-MTDATA(30 nm)/**7,8,9,10** (20 nm)/PBD(10 nm)/TPBi(25 nm)/Ca(10 nm)/Al(60 nm) (marked as devices A,B,C, and D, respectively). To achieve the high charge-balance the multilayer architectures of OLEDs were chosen (**Figure S4**). In such devices, molybdenum trioxide (MoO$_3$) was used for the preparation of hole-injection layers; 4,4′,4′′-tris[3-methylphenyl(phenyl)amino]triphenylamine (*m*-MTDATA) was employed for the fabrication of hole-transporting and electron-blocking layers, 2-(4-biphenylyl)-5-phenyl-1,3,4-oxadiazole (PBD) was used for the preparation of electron-transporting and hole-blocking layers and 1,3,5-tris(*N*-phenylbenzimidazol-2-yl)benzene (TPBi) was utilized for the preparation of electron-injection layers. Owing to the additional layers, the charge carrier barriers between work functions of the electrodes (ITO, Ca) and the molecular orbitals of light-emitting layers (**7-10)** were reduced (**Figure S4**).

The electroluminescence (EL) spectra of the devices A-D coincided with the photoluminescence (PL) spectra of solid films of emitters **7-10** (**Figure 5** and **9**). The electroluminescence characteristics of the non-doped electroluminescent devices ITO/MoO$_3$/m-MTDATA/**7-10**/PBD/TPBi/Ca/Al are shown in **Figure S5 a-d** and are summarized in **Table 5**. The turn-on voltages (V$_{on}$) of the devices were found to be in the range from 4.0 to 5.5 V at the brightness of 1 cd/m^2, while the maximum brightness was recorded in the range from 130 to 750 cd/m^2 at the driving voltage of 10 V. These parameters are comparable with those of the fluorescent deep blue OLEDs [44,45], however, the efficiencies of the devices were rather low (the maximal current, power, and external quantum efficiencies were lower than 1.3 cd/A, 0.8 lm/W, 0.95 %, respectively (**Figure S5 b-d**)). Commission Internationale de l'Eclairage (CIE) chromaticity coordinates (x,y) for the devices based on non-doped emitting layers **7**, **8**, **9**, and **10**, were found to be (0.183, 0.162), (0.265, 0.25), (0.19, 0.184), and (0.166, 0.133) respectively, which correspond to the blue colour. We note that the potential of the studied compounds was not fully disclosed in the non-doped blue electroluminescent devices. The efficiencies of non-doped blue electroluminescent devices will apparently be increased when appropriate auxiliary materials are available.
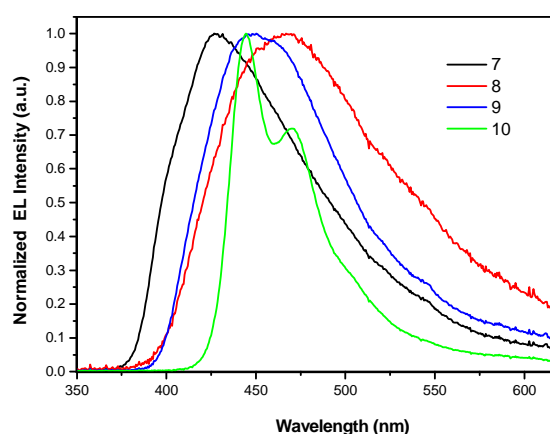

Figure 9. Electroluminescence spectra of the devices based on the non-doped emitting layers of **7-10**.

Table 5. EL characteristics of the fabricated devices.

Device	V_{on} at 1 Cd/m², V	Max brightness, cd/m²	Current efficiency, cd/A	Power efficiency, lm/W	External quantum efficiency, %	CIE 1931 UCS coordinates, (x,y)
					max	
A	5.5	750	1.3	0.8	0.95	(0.183;0.162)
B	4.5	270	0.06	0.03	0.03	(0.265;0.250)
C	4.0	140	1.15	0.8	0.75	(0.190;0.184)
D	4.0	130	0.97	0.64	0.7	(0.166;0.133)
AI	4.8	1970	4	1.5	1.75	(0.275;0.467) [a]
AII	5.1	6130	5.3	1.7	2.9	(0.468;0.381) [a]
DI	2.6	870	0.58	0.53	0.24	(0.324;0.289) [a]
DII	2.5	1300	0.56	0.53	0.24	(0.207;0.268) [a]

[a] – the values were taken at applied voltage of 8 V.

To increase the efficiencies of devices, doped light-emitting layers were used with the most promising emitters **7** and **10** which allowed to obtain the blue colour devices with higher efficiencies, while m-MTDATA and 4,4′-cyclohexylidenebis[*N*,*N*-bis(4-methylphenyl)benzenamine] (TAPC) were additionally utilized as the hosts. As CIE chromaticity coordinates for the devices based on non-doped emitting layers from **7** and **10** ((0.183, 0.162) and (0.166, 0.133), respectively) were related to the deeper blue colour than those devices based on non-doped emitting layers from **8** and **9** ((0.265, 0.25) and (0.19, 0.184), respectively), the compounds **7** and **10** were chosen for the fabrication of the white OLEDs. Electroluminescent devices based on doped light-emitting layers with the following architectures were fabricated: ITO/MoO₃(3 nm)/m-MTDATA(30 nm)/ TAPC:**7**, m-MTDATA:**7**, TAPC:**10** or m-MTDATA:**10** (20 nm)/PBD(10 nm)/TPBi(25 nm)/Ca(10 nm)/Al(60 nm) (marked as devices AI, AII, DI and DII). Low-energy bands with the maxima at 585 nm for the devices AI and DI and at 540 nm for the devices AII and

26

DII were additionally observed in the electroluminescence spectra of the doped OLEDs as compared to the spectra of the non-doped OLEDs (**Figure 10 a,b** and **Figure S6 a,b**). Appearance of the additional band can apparently be explained by the formation of the dimeric excited states (e.g. exciplexes or electroplexes) either in the doped light-emitting layers or at the interfaces between the layers of OLEDs due to the cross-interaction between the holes of donor and the electrons of acceptor [3]. To prove this assumption, PL spectra of the film of the molecular mixtures of the hosts and emitters were recorded (**Figure S7**). The PL spectra of the mixtures TAPC:**7**, m-MTDATA:**7**, TAPC:**10** and m-MTDATA:**10** were very similar to the PL spectra of pure **7** or **10** and did not contain bands at the wavelengths close to those of the low energy bands observed in EL spectra of the doped OLEDs (**Figure S7**). The similarity of shapes and positions of the PL spectra of the mixtures to the PL spectra of the pure emitters **7** or **10** indicates effective energy transfer from hosts to emitters. In addition, the PL spectra of the mixtures m-MTDATA:PBD and TAPC:PBD were found to be different as compared with the PL spectra of the pure m-MTDATA, TAPC, or PBD. The maximum at 540 nm of the PL spectrum of m-MTDATA:PBD film was found to be at the similar wavelength as the maximum of the additional band in the EL spectra of the devices AII and DII with m-MTDATA as the host. The PL decay curves of the film of the mixture m-MTDATA:PBD mixture recorded at the wavelength of maximum were well fitted by double-exponential function (**Figure S8 a**). The shorter lived component is most probably related to the monomeric fluorescence, while the longer lived component is apparently related to the exciplex emission which occurred due to the reverse intersystem crossing (RISC) from the singlet to the triplet state [46]. Therefore, the low-energy emission band in EL spectra of the doped OLEDs with the m-MTDATA host can be ascribed to the interface exciplex between m-MTDATA and PBD. Despite the exciplex emission with the maximum at 490 nm between TAPC and PBD observed in PL spectrum of the molecular mixture (**Figure S7** and **Figure S8 b**), the exciplex TAPC:PBD was not observed in the EL spectra of the devices AI and DI. The possible origin of electroluminescence

in low-energy region (585 nm) of the devices AI and DI is apparently the formation of electroplexes between TAPC and **7** (**10**) which only occurs under the electric fields. The similar electroplex emission between TAPC and a bipolar transporting material 2,6-bis(3-(carbazol-9-yl) phenyl)pyridine was observed previously [47].
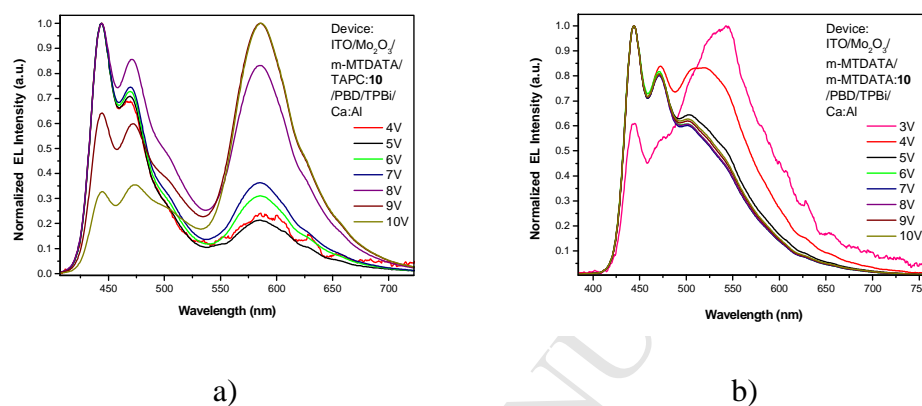

Figure 10. Electroluminescence spectra of the devices based on the doped emission layers TAPC:**10** (a) and m-MTDATA:**10** (b).

Commission Internationale de l'Eclairage (CIE) chromaticity coordinates (x,y) of the TAPC:**10** based device at voltages from 8 V to 9 V was found to be very close to the white point (0.33, 0.33) (**Figure S9**) due to the mixed blue monomer emission and orange electroplex emission in the TAPC:**10** emitting-layer. The current density–voltage–luminance and efficiencies versus current density characteristics for the doped devices are plotted in **Figure 11** and **Figure S10**. Improved maximal current of 4 and 5.3 cd/A, power of 1.5 and 1.7 lm/W, and external quantum of 1.75 and 2.9 % efficiencies were achieved for the devices AI and DI respectively (**Table 5**).
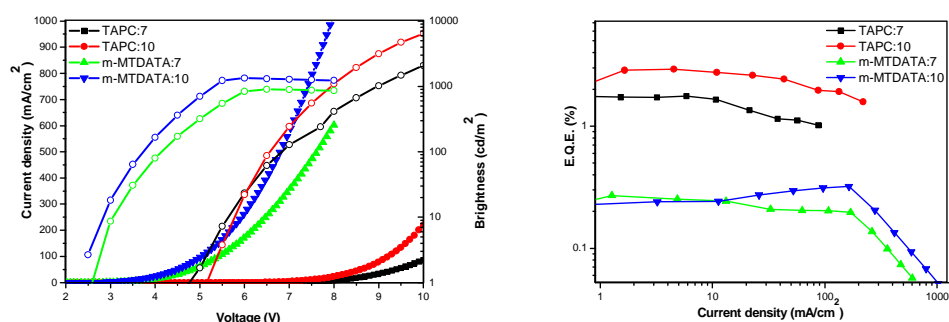
28

Figure 11. Current density−voltage and luminance−voltage characteristics of OLEDS based on the doped light-emitting layer TAPC:**7**, m-MTDATA:**7**, TAPC:**10** and m-MTDATA:**10** (a); external quantum efficiencies of the devices (b).

4. Conclusions

Four bipolar phenanthroimidazole-based derivatives containing carbazolyl and diphenylamino substituents were synthesized and characterized. The thermal, photophysical, photoelectrical and electrochemical properties of the obtained compounds were studied. It was concluded that new synthesised materials possess extremely high thermal stability (5% weight loss reaches 500°C) and form glasses with high glass transition temperatures ranging from 183 to 239 ^{o}C. Synthesised derivatives are efficient solid state blue-emissive materials with photoluminescence quantum yields ranged from 0.27 to 0.55. The electron photoemission spectra of the synthesized compounds were recorded and ionization potentials of 5.15-5.31 eV were established. It was found that synthesised phenanthroimidazoles derivatives are bipolar materials with well-balanced charge transport properties. Room temperature hole-drift mobilities established by time-of-flight technique reached 1.41×10^{-4} cm^2/V·s at an electric field of 2.96×10^{-6} cm^2/V·s and electron-drift mobility approached 1.68×10^{-4} cm^2/V·s at an electric field of 2.71×10^{-6} cm^2/V·s. Blue emitting OLEDs with CIE chromaticity coordinates of (0.183, 0.162), (0.265, 0.25), (0.19, 0.184), and (0.166, 0.133) have been prepared using phenanthroimidazole-based derivatives for non-doped emitting layers. In addition, the electroplex formation of the synthesized compounds was observed in a host:guest emitting layers with 4,4′-cyclohexylidenebis[*N*,*N*-bis(4-methylphenyl)benzenamine]. Two phenanthroimidazole-based derivatives were used for the fabrication of white OLEDs which were

29

based on both fluorescence and either electroplex or exciplex emissions. The best almost white device was characterized by maximal current efficiency of 5.3 cd/A, power efficiency of 1.7 lm/W, and external quantum efficiency of 2.9 %.

Acknowledgment

AUTHOR INFORMATION

Corresponding Author

*E-mail address: ramunas.lygaitis@ktu.lt (Ramunas Lygaitis).

Appendix A. Supplementary data

Supplementary data related to this article can be found at http://dx.doi.org/

References

[1] Goushi K, Yoshida K, Sato K, Adachi C. Organic light-emitting diodes employing efficient reverse intersystem crossing for triplet-to-singlet state conversion. Nat Photonics 2012; 6:253–8.

[2] Cherpak V, Stakhira P, Minaev B, Baryshnikov G, Stromylo E, Helzhynskyy I, et al. Mixing of phosphorescent and exciplex emission in efficient organic electroluminescent devices. ACS Appl Mater Interfaces 2015; 7:1219–25.

[3] Kalinowski J. Excimers and exciplexes in organic electroluminescence. Mater Sci Pol 2009; 27:735–56.

[4] Hung W-Y, Fang G-C, Lin S-W, Cheng S-H, Wong K-T, Kuo T-Y, et al. The first tandem, all-exciplex-based WOLED. Scientific Reports 2014; 4:5161.

[5] Cherpak V, Stakhira P, Minaev B, Baryshnikov G, Stromylo E, Helzhynskyy I, et al. Efficient "warm-white" OLEDs based on the phosphorescent bis-cyclometalated iridium(III) complex. J Phys Chem C 2014; 118:11271–8.

[6] Uoyama H, Goushi K, Shizu K, Nomura H, Adachi C. Highly efficient organic light-emitting diodes from delayed fluorescence. Nature 2012; 492:234–8.

[7] Hung W-Y, Fang G-C, Chang Y-C, Kuo T-Y, Chou P-T, Lin S-W, et al. Highly efficient bilayer interface exciplex for yellow organic light-emitting diode. ACS Appl Mater Interfaces 2013; 5:6826–31.

[8] Michaleviciute A, Gurskyte E, Volyniuk D, Cherpak V-V, Sini G, Stakhira P-Y, et al. Star-shaped carbazole derivatives for bilayer white organic light-emitting diodes combining emission from both excitons and exciplexes. J Phys Chem C 2012; 116:20769–78.

[9] Zhang T, Zhao B, Chu B, Li W, Su Z, Liu C, et al. Simple structured hybrid WOLEDs based on incomplete energy transfer mechanism: from blue exciplex to orange dopant. Scientific Reports 2015; 5:10234–41.

[10] Cherpak V, Gassmann A, Stakhira P, Volyniuk D, Grazulevicius J-V, Michaleviciute A, et al. Three-terminal light-emitting device with adjustable emission color. Org Electron 2014; 15:1396–400.

[11] Nakanotani H, Furukawa T, Morimoto K, Adachi C. Long-range coupling of electron-hole pairs in spatially separated organic donor-acceptor layers. Sci Adv 2016; 2:e1501470 1–7.

[12] Angioni E, Chapran M, Ivaniuk K, Kostiv N, Cherpak V, Stakhira P, et al. A single emitting layer white OLED based on exciplex interface emission. J Mater Chem C 2016; 4:3851–6.

[13] Zhang M, Chen Z, Xiao L, Qu B, Gong Q. High-color-quality white top-emitting organic electroluminescent devices based on both exciton and electroplex emission. Appl Phys Express 2011; 4:082105 1–3.

[14] Hao Y, Meng W, Xu H, Wang H, Liu X, Xu B. White organic light-emitting diodes based on a novel Zn complex with high CRI combining emission from excitons and interface-formed electroplex. Org Electron 2011; 12:136–42.

[15] Wen L, Li F, Xie J, Wu C, Zheng Y, Chen D, et al. Electroplex emission at PVK/Bphen interface for application in white organic light-emitting diodes. J Lumin 2011; 131:2252–4.

[16] Wang Z, Lu P, Chen S, Gao Z, Shen F, Zhang W, et al. Phenanthro[9,10-d]imidazole as a new building block for blue light emitting materials. J Mater Chem 2011; 21:5451–6.

[17] (a) Wang Z, Li X, Xue K, Li H, Zhang X, Liu Y, et al. Towards stable deep-blue emission and low efficiency roll-off in OLEDs based on phenanthroimidazole dimers. J Mater Chem C 2016; 4:1886–94;

(b) Wang Z, Li X, Zhang W, Zhang S, Li H, Yu Z, et al. The effect of meta coupling on colour purity, quantum yield, and exciton utilizing efficiency in deep-blue emitters from phenanthroimidazole isomers. Phys Chem Chem Phys 2015; 17:31894–901;

(c) Tang X, Bai Q, Peng Q, Gao Y, Li J, Liu Y, et al. Efficient deep blue electroluminescence with an external quantum efficiency of 6.8% and CIEy < 0.08 based on a phenanthroimidazole–sulfone hybrid donor–acceptor molecule. Chem Mater 2015; 27(20):7050–7;

(d) Chen S, Wu Y, Zhao Y, Fang D. Deep blue organic light-emitting devices enabled by bipolar phenanthro[9,10-d]imidazole derivatives. RSC Adv 2015; 5:72009–18;

(f) Qin W, Yang Z, Jiang Y, Lam J-W-Y, Liang G, Kwok H-S, et al. Construction of efficient deep blue aggregation-induced emission luminogen from triphenylethene for nondoped organic light-emitting diodes. Chem Mater 2015; 27:3892–901;

(g) Wang Z, Feng Y, Zhang S, Gao Y, Gao Z, Chen Y, et al. Construction of high efficiency non-doped deep blue emitters based on phenanthroimidazole: remarkable substitution effects on the excited state properties and device performance. Phys Chem Chem Phys 2014; 16:20772–9;

(h) Wang Z, Feng Y, Li H, Gao Z, Zhang X, Lu P, et al. Dimeric phenanthroimidazole for blue electroluminescent materials: the effect of substituted position attached to biphenyl center. Phys Chem Chem Phys 2014; 16:10837–43;

(i) Yuan Y, Chen J, Lu F, Tong Q, Yang Q, Mo H, et al. Bipolar phenanthroimidazole derivatives containing bulky polyaromatic hydrocarbons for nondoped blue electroluminescence devices with high efficiency and low efficiency roll-off. Chem Mater 2013; 25:4957–65;

(j) Zhang Y, Lai S-L, Tong Q-X, Lo M-F, Ng T-W, Chan M-Y, et al. High efficiency nondoped deep-blue organic light emitting devices based on imidazole-π-triphenylamine derivatives. Chem Mater 2012; 24:61–70.

[18] Liu H, Bai Q, Yao L, Zhang H, Xu H, Zhang S, et al. Highly efficient near ultraviolet organic light emitting diode based on a meta-linked donor– acceptor molecule. Chem Sci 2015; 6:3797–804.

[19] Li W, Lin W, Wang J, Guan X. Phenanthro[9,10-d]imidazole-quinoline boron difluoride dyes with solid-state red fluorescence. Org Lett 2013; 15(7):1768–71.

[20] Williams A-T-R, Winfield S-A, Miller J-N. Relative fluorescence quantum yields using a computer-controlled luminescence spectrometer. Analyst 1983; 108:1067–71.

[21] Lygaitis R, Schmaltz B, Degutyte R, Grazulevicius J-V, Degbia M, Strohriegl P, et al. Star-shaped triphenylamine-based molecular glass for solid state dye sensitized solar cell application. Synth Met 2014; 195:328–34.

[22] Miyamoto E, Yamaguchi Y, Yokoyama M. Ionization potential of organic pigment film by atmospheric photoelectron emission analysis. Electrophotography 1989; 28:364 Electrophotography 1989; 28:364–70.

[23] Lygaitis R, Matoliukstyte A, Kreiveniene N, Grazulevicius J-V. Synthesis and photophysical properties of bipolar low-molar-mass amorphous materials. J Photochem Photobiol A 2004; 167:163–8.

33

[24] Tse S-C, Cheung C-H, So S-K. Organic electronics. Materials, processing, devices and applications. In: So F, editors. Charge transport and injection in amorphous organic semiconductors. New York: Taylor & Francis Group, p.71–4.

[25] Mimaite V, Grazulevicius J-V, Laurinaviciute R, Volyniuk D, Jankauskas V, Sini G. Can hydrogen bonds improve the hole-mobility in amorphous organic semiconductors? Experimental and theoretical insights. J Mater Chem C 2015; 3:11660–74.

[26] Kohn W, Sham L. Self-consistent equations including exchange and correlation effects. Phys Rev 1965; 140:A1133.

[27] (a) Lee C-T, Yang W-T, Parr R-G. Development of the Colle-Salvetti correlation-energy formula into a functional of the electron density. Phys Rev B 1988; 37:785–9;

(b) Becke A-D. Density☐functional thermochemistry. III. The role of exact exchange. J Chem Phys 1993; 98:5648–52.

[28] Frisch M-J, Trucks G-W, Schlegel H-B, Scuseria G-E, Robb M-A, Cheeseman J-R, et al. Gaussian 09, Revision B.01. Wallingford CT: Gaussian, Inc; 2009.

[29] (a) Casida M-E, Jamorski C, Casida K-C, Salahub D-R. Molecular excitation energies to high-lying bound states from time-dependent density-functional response theory: Characterization and correction of the time-dependent local density approximation ionization threshold. J Chem Phys 1998; 108:4439–49;

(b) Bauernschmitt R, Ahlrichs R. Treatment of electronic excitations within the adiabatic approximation of time dependent density functional theory. Chem Phys Lett 1996; 256: 454-64;

(c) Gross E-K-U, Kohn W. Time-dependent density-functional theory. Adv Quantum Chem 1990; 21: 255–91;

(d) Gross E-K-U, Kohn W. Local density-functional theory of frequency-dependent linear response. Phys Rev Lett 1985; 55: 2850–2;

(e) Runge E, Gross E-K-U. Density-functional theory for time-dependent systems. Phys Rev Lett 1984; 52:997–1000.

[30] Brédas J-L, Beljonne D, Coropceanu V, Cornil J. Charge-transfer and energy-transfer processes in π-conjugated oligomers and polymers: a molecular picture. Chem Rev 2004; 104: 4971–5004.

[31] Ciszek J-W, Tour J-M. Synthesis of ladder polyaromatics as new molecular device candidates. Tet Lett 2004; 45:2801–3.

[32] Callahan R, Marshall K, Rothchild R, Rosmarion K. Syntheses of phencyclone analogues. applications for NMR studies of hindered rotations and magnetic anisotropy in crowded Diels–Alder adducts. Chem Educator 2001; 6:227–34.

[33] Ullman F. Uber eine neue bildungsweise von diphenylaminderivativen. Ber B 1903; 36:2382–5.

[34] Wolfe J-P, Buchwald S-L. Palladium-catalyzed amination of aryl iodides. J Org Chem 1996; 61:1133–5.

[35] Zhuang S, Shangguan R, Jin J, Tu G, Wang L, Chen J, et al. Efficient nondoped blue organic light-emitting diodes based on phenanthroimidazole-substituted anthracene derivatives. Org Electron 2012; 13:3050–9.

[36] Wang K, Sun P, Xu H, Li J, Wang F, Miao Y, et al. Two novel bipolar compounds based-on 1, 2, 4-triazol derivatives for non-doped deep-blue and green phosphorescent OLED applications. Dyes Pigm 2017; 43:25-32.

[37] Xu H, Sun P, Wang K, Li J, Wang F, Miao Y, et al. Bipolar hosts and non-doped deep-blue emitters (CIEy = 0.04) based on phenylcarbazole and 2-(2-phenyl-2H-1,2,4-triazol-3-yl)pyridine groups. J Mater Chem C 2017; 5:4455-62.

[38] (a) Luo J-D, Xie Z-L, Lam J-W-Y, Cheng L, Chen H-Y, Qiu C-F, et al. Aggregation-induced emission of 1-methyl-1,2,3,4,5-pentaphenylsilole. Chem Commun 2001; 18:1740–1;

(b) Chen J-W, Xu B, Yang K-X, Cao Y, Sung H-H-Y, Williams Y-D, et al. Photoluminescence spectral reliance on aggregation order of 1,1-Bis(2′-thienyl)-2,3,4,5-tetraphenylsilole. J Phys Chem B 2005; 109:17086–93;

(c) Lim S-J, An B-K, Jung S-D, Chung M-A, Park S-Y. Photoswitchable organic nanoparticles and a polymer film employing multifunctional molecules with enhanced fluorescence emission and bistable photochromism. Angew Chem Int Ed 2004; 43:6346–50;

(d) Yeh H-C, Yeh S-J, Chen C-T. Readily synthesised arylamino fumaronitrile for non-doped red organic light-emitting diodes. Chem Commun 2003; 9 (20):2632–3.

[39] Borsenberger P-M, Shi J. Hole transport in a vapor deposited phenylenediamine molecular glass. Phys Stat Sol B 1995; 191 (2):461–9.

[40] Bucinskas A, Volyniuk D, Danyliv Y, Grazulevicius J-V, Baryshnikov G, Minaev B, et al. N-annelated perylenes as effective green emitters for OLEDs. RSC Adv 2015; 5:78150–9.

[41] Marcus R-A. On the theory of oxidation-reduction reactions involving electron transfer. J Chem Phys 1956; 24(5):966–78.

[42] Marcus R-A. Electron transfer reactions in chemistry. Theory and experiment. Rev Mod Phys 1993; 65(3):599–610.

[43] Marcus R-A, Sutin N. Electron transfers in chemistry and biology. Biochim Biophys Acta 1985; 811(3):265–322.

[44] Jou J-H, Kumar S, Fang P-H, Venkateswararao A, Thomas K-R-J, Shyue J-J, et al. Highly efficient ultra-deep blue organic light emitting diodes with a wet- and dry-process feasible cyanofluorene acetylene based emitter. J Mater Chem C 2015; 3:2182–94.

[45] Yang X, Xu X, Zhou G. Recent advances of the emitters for high performance deep-blue organic light-emitting diodes. J Mater Chem C 2015; 3:913–44.

[46] Zhang T, Chu B, Li W, Su Z, Peng Q-M, Zhao B, et al. Efficient triplet application in exciplex delayed fluorescence OLEDs using a reverse intersystem crossing mechanism based on a ΔES-T of around zero. ACS Appl Mater Interfaces 2014; 6:11907–14.

[47] Chen D, Wang Z, Wang D, Wu Y-C, Lo C-C, Lien A, et al. Efficient exciplex organic light-emitting diodes with a bipolar acceptor. Org Electron 2015; 25:79–84.

Highlights

- Solid-state blue emission with quantum yields reaching 0.55

- Balanced bipolar charge mobilities

- Application in blue and white emitting OLEDs